Robust Design Optimization of SPMSM for Robotic Actuator Considering Assembly Imperfection of Segmented Stator Core

Soo-Gyung Lee, Saekyeol Kim, Jin-Cheol Park, Min-Ro Park, Tae Hee Lee, *Member, IEEE*, and Myung-Seop Lim, *Member, IEEE*

***Abstract*—To be used as a robotic actuator, a surface-mounted permanent magnet synchronous motor (SPMSM) requires a low cogging torque characteristic. The aim of this study is to analyze and reduce the cogging torque's variation due to the assembly imperfection of the segmented stator that is widely used in the SPMSM. Considering the interconnection of the stator segments, an equivalent modeling method of the segmented stator with assembly imperfection is introduced. In addition, the variation in the cogging torque caused by the assembly imperfection is mathematically evaluated. Then, a robust design process that incorporates a sensitivity analysis and a robust design optimization is proposed. By using the proposed design, a robust optimum design model was built and its validity was verified through Monte Carlo simulation and tests.**

***Index Terms*—Assembly imperfection, manufacturing tolerance, robotic actuator, robust design optimization, segmented stator, sensitivity analysis.**

I. Introduction

INDUSTRIAL robots involve complex operating conditions at various loads. Thus, small, lightweight, and low-friction robotic actuators are required for precise and fast motion control under repeated acceleration and deceleration [1]. Hence, surface-mounted permanent-magnet synchronous motors (SPMSMs) are widely used as robotic actuators [2], Moreover, a segmented stator is employed in the SPMSMs for robotic actuators, yielding high-productivity, and high-fill factor of windings [3].

However, SPMSMs with the segmented stator exhibit problems with respect to cogging torque, which is produced by the interaction between the magneto-motive force harmonics of the permanent-magnet (PM) and the air-gap permeance harmonics. The cogging torque causes torque ripples, vibration, and noise [4]. In industrial robot applications, the cogging torque of the robot actuators can create many problems. According to [5], the haptic perception of a robot is easily affected by the cogging torque, especially at low torques. In [6], it is mentioned that vibration can be generated in a robot while accelerating, if the cogging torque exists. According to [7], the cogging torque deteriorates the back-drivability related to motion control of a robot.

To reduce cogging torque, many studies focused on devising a design method. This is because cogging torque is significantly affected by the shape of the motor [4]. In general, at the stator side, the slot-opening width and tooth tip are optimized for reducing cogging torque [8]. Furthermore, skewing and teeth notching are applied to reduce the cogging torque. At the rotor side, in addition to pole-angle and PM-shaping optimization, skewing and notching poles are used [9]. However, even with the use of such methods in the motor-design stage, a high cogging torque could be generated in mass-produced SPMSMs [10]. This is because of the difficulty in preventing unwanted tolerances while mass producing SPMSMs and the sensitivity of cogging torque to such tolerances.

Many researchers have studied the effects of manufacturing tolerances on the cogging torque of PM motors. In [11] and [12], the causes of the occurrence of additional harmonic components (AHCs) of the cogging torque were investigated. Stator tolerances are known to produce AHCs whose frequencies are multiples of pole number, while rotor tolerances produce the AHCs whose frequencies are multiples of the number of slots.

Among the many causes of tolerance generation, this paper focused on the assembly imperfection of the segmented stator. This is because various stator tolerances are produced during the assembly of the segmented stator. According to [13]–[16], the additional stator-gaps between the stator segments are known to produce AHCs in the cogging torque. Other researchers investigated the effect of tooth-bulges occurring during the assembly of the stator segments, assuming that a tooth-bulge of one segment did not affect tooth-bulges of adjacent segments [17], [18]. However, considering the practical assembly process of the segmented stator, a tooth-bulge in one segment may affect tooth-bulges in adjacent segments. This is because the segments are interconnected

Considering the interconnection between the segments, an equivalent modeling method for the segmented stator is

Manuscript received January 14, 2020; revised April 21, 2020; accepted May 24, 2020. Date of publication June 1, 2020; date of current version November 24, 2020. This work was supported in part by the National Research Foundation of Korea(NRF) and in part by the Korea government (MSIP; Ministry of Science, ICT & Future Planning) (No. 2018R1C1B5085447). Paper no. TEC-00046-2020. *(Corresponding author: Myung-Seop Lim.)*

Soo-Gyung Lee, Saekyeol Kim, Jin-Cheol Park, Tae Hee Lee, and Myung-Seop Lim are with the Hanyang University, Seoul 04763, South Korea (e-mail: sgar1109@hanyang.ac.kr; kyeol8805@gmail.com; skensk1990@hanyang.ac.k; thlee@hanyang.ac.kr; myungseop@hanyang.ac.kr).

Min-Ro Park is with the Korea Institute of Robotics & Technology Convergence, Pohang, Republic of Korea (e-mail: minro@kiro.re.kr).

Color versions of one or more of the figures in this article are available online at https://ieeexplore.ieee.org.

Digital Object Identifier 10.1109/TEC.2020.2999127

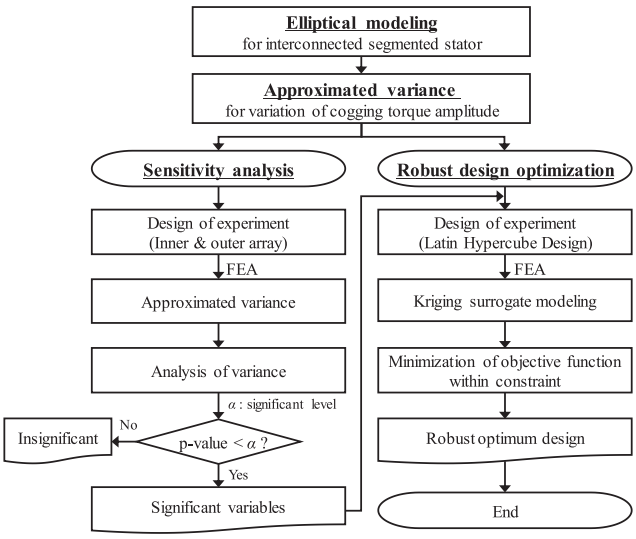

Fig. 1. Framework of this study.

proposed in this paper. In addition, we investigated the effects of the stator assembly imperfection on the cogging torque, and devised a robust motor design to reduce these effects.

The contributions of this study to the literature are as follows:

1) elliptical modeling for segmented stator,
2) approximated variance cogging torque variation,
3) sensitivity analysis of cogging torque variation,
4) robust design optimization (RDO),
5) verification using Monte Carlo simulation (MCS) and comparison with test results.

First, the elliptical modeling for the segmented stator is proposed. Through this modeling, various stator tolerances are well reflected in a model, considering the interconnection between the stator segments. In addition, design parameters with uncertainties are defined, which are related to shape of trajectory consisting of the stator's inner radii.

Second, the variation in the amplitude of the cogging torque due to the imperfection in the stator assembly is mathematically evaluated by defining the approximated variance.

Third, a sensitivity analysis method for the variation in the cogging torque amplitude is proposed, and the statistical significance of design variables is determined for the variation.

Fourth, an RDO is conducted to reduce the effects of the assembly imperfection of the stator on the cogging torque. Subsequently, a robust optimum design model was determined that ensures a small cogging torque even if tolerances are produced in the segmented stator.

Finally, the validity of the robust optimum design model is confirmed using the MCS [19], [20]. Four prototypes of the robust optimum design model were fabricated, and their cogging torque test results were compared with the cogging torque distribution estimated using the MCS.

Accordingly, this study offers motor designers with an overall robust design procedure that is necessary for the mass production of motors such as robotic actuators. Fig. 1 shows the framework of this study.

TABLE I
HARMONIC COMPONENTS OF COGGING TORQUE ACCORDING TO CAUSES

	Harmonic components		
	Native	Additional	
Cause	Interaction of PM and slot	Stator tolerances	Rotor tolerances
Fundamental frequency	LCM($2p$,S)	$2p$	S

II. ASSEMBLY IMPERFECTION OF SEGMENTED STATOR

A 16-pole-18-slot SPMSM conventional model for a robotic actuator was analyzed. First, a prototype of the conventional model was fabricated, and its cogging torque was experimentally tested. In addition, finite-element-analysis (FEA) simulation was conducted without considering all manufacturing tolerances. By comparing the test and simulation results, the effects of the tolerances on the cogging torque are discussed. To investigate which tolerance is produced owing to the stator assembly imperfection, the inner radius in each segment of the prototype was measured. Then, an equivalent modeling method for the segmented stator is proposed. Accordingly, the stator tolerances could be well reflected in the simulation model, considering the interconnection between the stator segments.

A. Harmonic Components of Cogging Torque

The harmonic components (HCs) of the cogging torque of a SPMSM are determined according to the number of poles and slots. The cogging torque of an ideal model, in which manufacturing tolerances are nonexistent, contains a native HC (NHC). However, owing to unwanted manufacturing tolerances, AHCs are produced in the cogging torque. With reference to [11], the NHC and AHCs of the cogging torque are presented in Table I, where p is the number of pole pairs and S is the number of slots. As the conventional model is a 16-pole-18-slot SPMSM, the NHC of the cogging torque of the conventional model was predicted to be 144th order. Moreover, AHCs of orders 16th and 18th were predicted to be caused by manufacturing tolerances in the stator and rotor, respectively.

To analyze the effects of the tolerances on the cogging torque of the conventional model, the cogging torque of the prototype was experimentally tested and an FEA simulation was conducted using a model without all the manufacturing tolerances. The simulation model is depicted in Fig. 2(a), and Fig. 2(b) shows the test set-up for the cogging torque of the prototype. A Sugawara cogging torque meter was used, which includes torque and angle sensors offering high sensitivity and small resolution. In this cogging torque meters, a sensor, an encoder, and a drive motor are axially aligned. The test motor shaft was coupled to the tester shaft that rotated at 1rpm. The cogging torque measurement accuracy was $\pm$ 1mNm, and the angle measurement accuracy was $\pm$ 1.5° per revolution.

Fig. 2(c) shows the test and simulation results of the cogging torque waveform. The peak-to-peak value of the cogging torque obtained through the test was higher than that obtained through the simulation. As shown in Fig. 2(d), AHCs were produced owing to the tolerances: the 16th and the 18th order AHCs were produced by stator and rotor tolerances, respectively. In this

Dimension	Value (mm)
PM width	9.3
PM thickness	4
Air-gap length	0.6
Teeth width	7.4
Yoke width	3.7

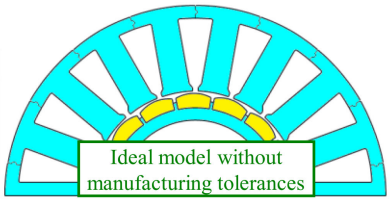

(a) FEA simulation model without manufacturing tolerances.

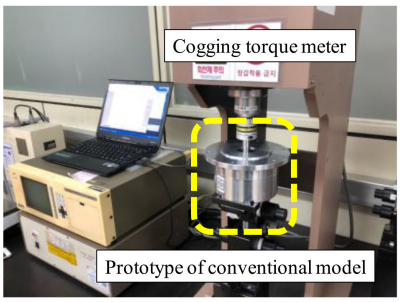

(b) Test set-up for the prototype.

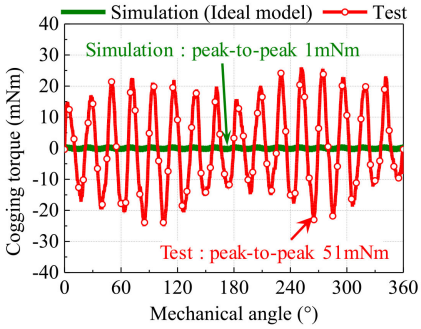

(c) Cogging torque waveform. (Test and simulation results.)

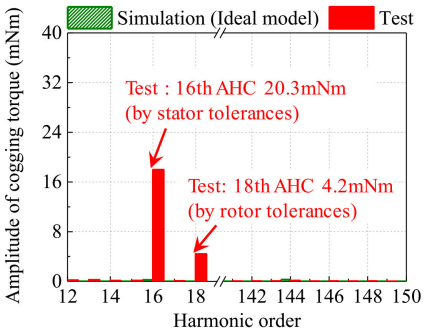

(d) Harmonic components of cogging torque. (Test and simulation results.)

Fig. 2. FEA simulation neglecting manufacturing tolerances and cogging torque test for the prototype of the conventional model.

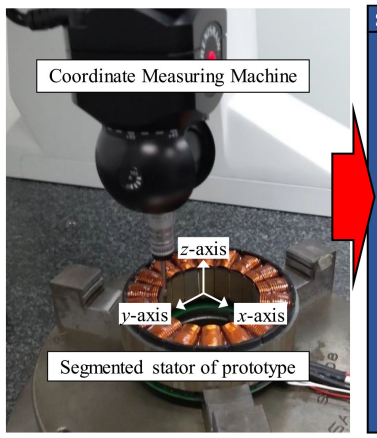

Segment	x-axis	y-axis	z-axis
1	29.11	-0.005	-10.19
2	27.36	9.95	-10.19
3	22.31	18.71	-10.19
4	14.56	25.21	-10.19
5	5.06	28.66	-10.19
6	-5.05	28.67	-10.19
7	-14.55	25.21	-10.19
8	-22.31	18.71	-10.19
9	-27.36	9.95	-10.19
10	-29.11	-0.004	-10.19
11	-27.36	-9.96	-10.19
12	-22.30	-18.71	-10.19
13	-14.54	-25.22	-10.19
14	-5.04	-28.67	-10.19
15	5.06	-28.67	-10.19
16	14.55	-25.21	-10.19
17	22.29	-18.72	-10.19
18	27.35	-9.96	-10.19

(a) Measurement set-up and raw data for inner radii of each segment.

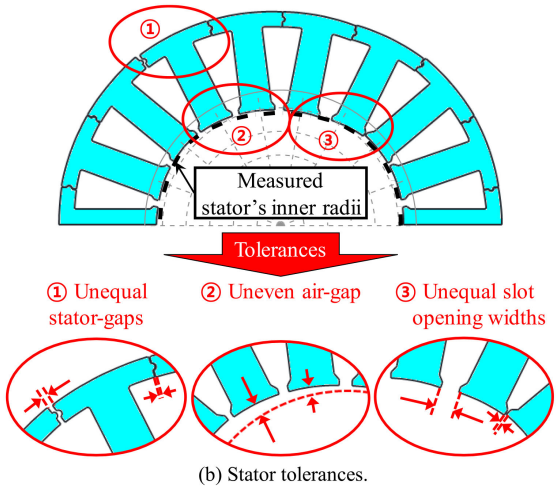

(b) Stator tolerances.

Fig. 3. Identification of stator tolerances caused by assembly imperfection of segmented stator in the prototype of the conventional model.

study, the focus is on the 16th AHC that is the largest among all the AHCs of the cogging torque.

B. Manufacturing Tolerances Due to Assembly Imperfection of Segmented Stator Considering An Interconnected Structure

As the stator segments are interconnected, radial distances of tooth-bulges may differ by each segment when the segments are imperfectly assembled. Consequently, various stator tolerances are produced while assembling the stator segments. As shown in Figs. 3(a) and (b), tolerances caused by the imperfection in the stator assembly were investigated by measuring the inner radii of each segment in the prototype of the conventional model. The inner radii of each segment were measured at the center of each segment. Fig. 3(a) shows the measurement set-up and raw data of the measured inner radii of the segments. The Renishaw coordinate measuring machine (CMM) was used as the measurement device. The repeatability of position was less than 0.4μm, and the accuracies of step spacing with respect to the theoretical positions were assured within $\pm$ 0.24mm. Assuming that the vertical angle error was nonexistent, the inner radii were measured at the constant z-axial position of each segment. As depicted in Fig. 3(b). three stator tolerances were identified: unequal stator-gaps, uneven air-gap, and unequal slot-opening width. These different types of tolerances occurred owing to the radial distances of the tooth-bulges different by the segments.

The cogging torque was then calculated through FEA simulation applying these tooth-bulges to the simulation model. Fig. 4 shows the comparison between the simulation and test results. Similar to the test result, a 16th order AHC was generated in the simulation result. Thus, the simulation result of the cogging torque waveform was similar to the test result.

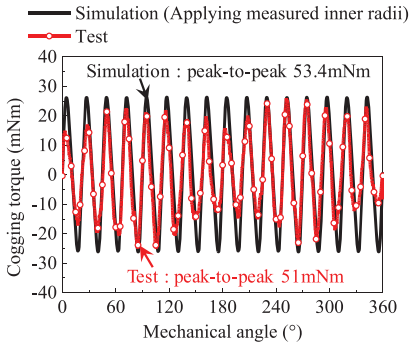

(a) Cogging torque waveforms. (Test and simulation results.)

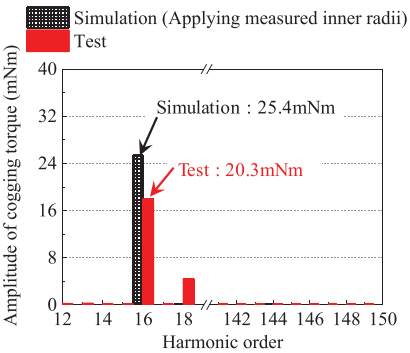

(b) Harmonic components of cogging torque. (Test and simulation results.)

Fig. 4. Cogging torque of the conventional model: test and FEA simulation applying measured inner radii.

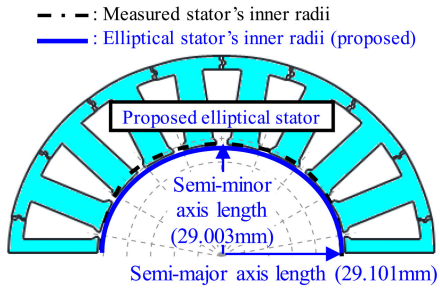

(a) Simulation model for segmented stator using elliptical modeling.

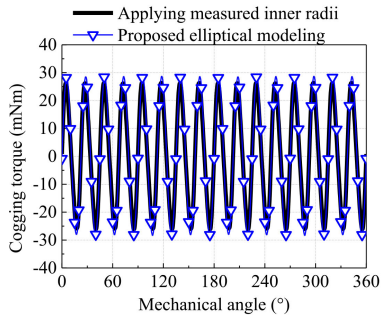

(b) Cogging torque waveform. (Simulation results.)

Fig. 5. FEA simulations depending on modeling methods of the segmented stator.

C. Proposed Elliptical Modeling for the Segmented Stator

Although the accuracy of predicting the cogging torque waveform by using the FEA simulation with the tooth-bulges was high enough, considerable amounts of time and effort are required to apply the various radial distances of the tooth-bulges to the simulation model. This section presents an elliptical modeling for the segmented stator, where the shape of the trajectory consisting of the stator's inner radii is affected by the imperfections in the stator assembly. Thus, two design parameters with uncertainties are defined: the semi-minor axis length, and the out of roundness which is the difference between the lengths of the semi-major and semi-minor axes.

Fig. 5(a) shows the segmented stator of the simulation model for the conventional model using the proposed elliptical modeling. The sizes for the ellipse formed by the trajectory of the stator's inner radii were decided according to the measurement results of the stator's inner radii; the semi-minor axis length was the same as the shortest radius, and the out of roundness was the same as the difference between the longest and shortest radii. Thus, the lengths of the semi-major and semi-minor axes of the stator's inner radii trajectory were the same as 29.101mm and 29.003mm, respectively.

Depending on the modeling methods, the cogging torque waveforms using FEA simulations are presented in Fig. 5(b). Although these waveforms are similar to each other, the proposed method enables much simpler modeling of the segmented stator while considering the interconnected structure.

III. Calculation of Cogging Torque Variation Caused by Assembly Imperfection of Segmented Stator

Owing to the stator assembly imperfection, various stator tolerances occur and the amplitude of the cogging torque varies. Statistically, this variation in the amplitude can be defined as the variance in the probability distribution of the cogging torque's amplitude. To estimate the variance in the probability distribution of the cogging torque's amplitude, several simulations or tests are typically required. However, conducting many simulations or tests entails high costs for computation, production, and measurement.

In this section, the approximated variance is defined based on Taylor expansion as in [21]. As assumptions, the elliptical modeling presented in Section II was applied to the segmented stator, and probabilities of the design parameters related to the stator's inner radii trajectory were assumed to form Gaussian distributions. At the nominal design point where the two design parameters with uncertainties are mean values, a function of the amplitude of the cogging torque was approximated according to an infinite sum of the function's derivatives:

$$f\left(x_{p1}, x_{p2}\right) \approx \mu_f + \sum_{i=1}^{2} \frac{\partial f\left(\mu_{x_{p1}}, \mu_{x_{p2}}\right)}{\partial x_{pi}} \left(x_{pi} - \mu_{x_{pi}}\right) + \cdots \tag{1}$$

where x_{p1} is the length of the semi-minor axis of the stator's inner radii trajectory and x_{p2} denotes the out of roundness of the stator's inner radii trajectory. When assuming the probability distributions of x_{p1} and x_{p2} as Gaussian distributions, $\mu_{x_{p1}}$ and$\mu_{x_{p2}}$ denote the mean values of x_{p1} and x_{p2}, respectively. In (1), f is the approximated function of the cogging torque's

amplitude and μ_f is the mean value of f, which is calculated through a simulation where values of x_{p1} and x_{p2} are the mean values.

Then, the variance of the amplitude of the cogging torque is formulated as:

$$\sigma_f^2\left(x_{p1}, x_{p2}\right) \approx \left\{\frac{\partial f\left(\mu_{x_{p1}}, \mu_{x_{p2}}\right)}{\partial x_{p1}}\right\}^2 \cdot \sigma_{x_{p1}}^2 + \left\{\frac{\partial f\left(\mu_{x_{p1}}, \mu_{x_{p2}}\right)}{\partial x_{p2}}\right\}^2 \cdot \sigma_{x_{p2}}^2 \quad (2)$$

where ${\sigma_f}^2$ denotes the approximated variance of the cogging torque amplitude. $\sigma_{x_{p1}}^2$ and $\sigma_{x_{p2}}^2$ are the variances of the Gaussian distributions of the semi-minor axis length and the out of roundness, respectively. In this study, we assumed that the manufacturing qualities of x_{p1} and x_{p2} are managed based on the six-sigma process. The partial derivatives in (2) are solved using the finite difference method, as follows:

$$\frac{\partial f\left(\mu_{x_{p1}}, \mu_{x_{p2}}\right)}{\partial x_{p1}} \approx \frac{f\left(\left(\mu_{x_{p1}} + h_1\right), \mu_{x_{p2}}\right) - f\left(\mu_{x_{p1}}, \mu_{x_{p2}}\right)}{h_1} \quad (3)$$

$$\frac{\partial f\left(\mu_{x_{p1}}, \mu_{x_{p2}}\right)}{\partial x_{p2}} \approx \frac{f\left(\mu_{x_{p1}}, \left(\mu_{x_{p2}} + h_2\right)\right) - f\left(\mu_{x_{p1}}, \mu_{x_{p2}}\right)}{h_2} \quad (4)$$

where h_1 and h_2 are increment values for x_{p1} and x_{p2}, respectively. The first term of the numerator on the right-hand side of (3) represents the value of the cogging torque amplitude calculated through a simulation, where the value of x_{p1} has been incremented by h_1 from the mean value. Similarly, the first term of the numerator on the right-hand side of (4) represents the value of the cogging torque amplitude calculated through a simulation, where the value of x_{p2} has been incremented by h_2 from the mean value. The second term of the numerator on the right-hand side of both (3) and (4) represents the value of the cogging torque amplitude calculated in a simulation, where both x_{p1} and x_{p2} are the mean values. To improve accuracy in the calculation of the derivatives, the values of h_1 and h_2 must be sufficiently small.

In this study, the variance calculated based on the Taylor expansion in (2) was termed as the approximated variance, which enables the quantitative evaluation of the cogging torque's variation due to the assembly imperfection of stator segments. The validity of the approximated variance was confirmed using MCS with more than 10^6 simulations to estimate the probability distribution of the cogging torque's amplitude. To efficiently conduct the several simulations, a kriging surrogate model of the cogging torque amplitude was built and used. Table II presents the approximated variance and the MCS variance of the conventional model. Compared with the MCS variance, the approximated variance has a reasonably small error of 1.5%. Therefore, the approximated variance was used in this study to investigate the sensitivity of the cogging torque variation and minimize the variation.

TABLE II
VERIFICATION OF APPROXIMATED VARIANCE USING MONTE CARLO SIMULATION

Conventional model		Value	Error
Variance of peak-to-peak value of cogging torque (mNm^2)	Approximated	276.2	1.5%
	Monte Carlo simulation	272.2	-

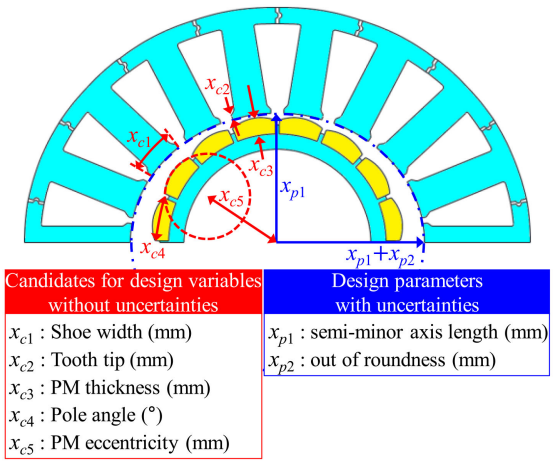

Fig. 6. Design parameters and candidates for design variables.

IV. SENSITIVITY ANALYSIS

This section presents a sensitivity analysis method for the variation in the amplitude of the cogging torque due to the assembly imperfection of the stator segments. The elliptical modeling in Section II was applied to the simulation model, and the approximated variance in Section III was employed for evaluating the variation in the amplitude of the cogging torque's HCs. Through the sensitivity analysis, the statistical significance of the candidates for design variables was identified.

A. Design of Experiment

In Fig. 6, five candidates for the design variables are depicted: shoe width x_{c1}, tooth tip x_{c2}, PM thickness x_{c3}, Pole angle x_{c4}, and PM eccentricity x_{c5}. The two design parameters with uncertainties relative to the stator's inner radii trajectory are also described: semi-minor axis length x_{p1}, and out of roundness x_{p2}.

Table III presents a design of experiment (DOE) table with inner and outer arrays proposed in this paper. The values from 0 to 2 indicate the levels of each design candidate and parameter. The values for the design candidates and parameters depending on their levels are presented in Table IV. The levels of the design candidates were determined according to their lower and upper boundaries. Moreover, the levels of the design parameters with uncertainties were determined to calculate the approximated variance. Thus, the differences between levels 0 and 1 of each design parameter are the same as the values of h_1 and h_2 in (3) and (4). In this study, the increments were set to 0.0001mm to ensure the high accuracy of derivatives calculations. In the inner array, the five candidates for design variables were placed based on the orthogonal array method [22]. The design parameters

TABLE III
PROPOSED DESIGN OF EXPERIMENT TABLE

DOE point	Inner array for candidates of design variables					Outer array for design parameters with uncertainties (stator tolerances)					
						First		Second		Third	
	x_{c1}	x_{c2}	x_{c3}	x_{c4}	x_{c5}	x_{p1}	x_{p2}	x_{p1}	x_{p2}	x_{p1}	x_{p2}
1	0	0	0	0	0	0	0	1	0	0	1
2	1	1	1	1	1	0	0	1	0	0	1
3	2	2	2	2	2	0	0	1	0	0	1
4	0	0	1	2	1	0	0	1	0	0	1
5	1	1	2	0	2	0	0	1	0	0	1
6	2	2	0	1	0	0	0	1	0	0	1
7	0	1	0	2	2	0	0	1	0	0	1
8	1	2	1	0	0	0	0	1	0	0	1
9	2	0	2	1	1	0	0	1	0	0	1
10	0	2	2	0	1	0	0	1	0	0	1
11	1	0	0	1	2	0	0	1	0	0	1
12	2	1	1	2	0	0	0	1	0	0	1
13	0	1	2	1	0	0	0	1	0	0	1
14	1	2	0	2	1	0	0	1	0	0	1
15	2	0	1	0	2	0	0	1	0	0	1
16	0	2	1	1	2	0	0	1	0	0	1
17	1	0	2	2	0	0	0	1	0	0	1
18	2	1	0	0	1	0	0	1	0	0	1

TABLE IV
VALUES OF CANDIDATES AND DESIGN PARAMETERS

Contents		Unit	Level		
			0	1	2
Candidates for design variables	Shoe width x_{c1}	(mm)	8.7	9.2	9.7
	Tooth tip x_{c2}	(mm)	0.50	1.25	2.00
	PM thickness x_{c3}	(mm)	2.0	3.0	4.0
	Pole angle x_{c4}	(°)	19.10	20.25	21.4
	PM eccentricity x_{c5}	(mm)	0.0	9.4	18.8
		Unit	Level		
			0		1
Design parameters with uncertainties (stator tolerances)	Semi-minor axis length of stator's inner trajectory x_{p1}	(mm)	29.1750		29.1751
	Out of roundness of stator's inner trajectory x_{p2}	(mm)	0.0750		0.0751

with uncertainties were located in the outer array to calculate the approximated variance at each DOE point. In the outer array, three rows are required for the design parameters with uncertainties. The first row indicates that design parameters x_{p1} and x_{p2} are the mean values. The second row indicates that x_{p1} is incremented as much as h_1 from its mean value, while x_{p2} remains the mean value. In the third row, x_{p2} is incremented as much as h_2 while x_{p1} remains the mean value.

At each DOE point, FEA models were constructed and the amplitudes of the cogging torque's HCs were computed. For the mean value of the cogging torque amplitude, the inner array and the first row of the outer array were used. By using (2)-(4), the approximated variance was calculated by employing the inner array and the three rows of the outer array. The mean and approximated variance values of the amplitudes of the 16th order AHC and 144th NHC are presented in Table V.

B. Analysis of Variance

For the 16th order AHC and 144th order NHC of the cogging torque, analysis of variance (ANOVA) was used to investigate the effects of the design candidates. Fig. 7 displays the *p*-values

TABLE V
SIMULATION RESULTS IN DESIGN OF EXPERIMENT TABLE

DOE point	Amplitude of 16th order additional harmonic component		Amplitude of 144th order native harmonic component	
	Mean (mNm)	Approximated variance (mNm^2)	Mean (mNm)	Approximated variance (mNm^2)
1	0.2	0.02	5.0	0.3
2	8.9	8.7	2.7	0.1
3	32.7	121.6	0.1	0.0004
4	1.0	0.1	0.08	0.004
5	4.5	1.8	5.4	0.6
6	3.5	63.9	3.1	0.1
7	12.6	18.7	0.05	0.04
8	25.5	71.7	9.3	1.1
9	0.7	0.1	1.6	0.009
10	22.6	53.9	7.5	0.4
11	0.5	0.04	1.1	0.04
12	13.2	23.5	0.1	0.01
13	12.2	16.4	2.1	0.1
14	30.2	107.5	0.3	0.01
15	2.4	1.0	4.9	0.4
16	23.7	61.6	1.0	0.04
17	1.2	0.2	0.09	0.001
18	5.6	4.1	7.5	0.9

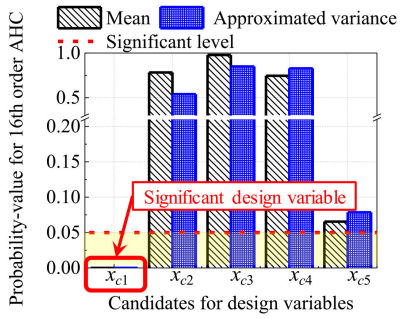

(a) 16th order additional harmonic component of cogging torque.

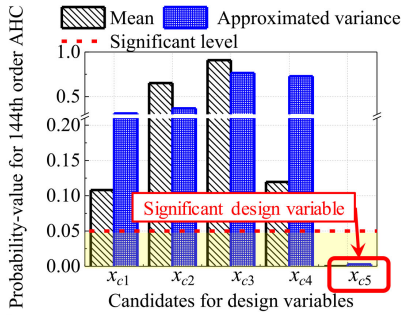

(b) 144th order native harmonic component of cogging torque.

Fig. 7. Sensitivity analysis results.

of the candidates for the design. Based on the *p*-values, the statistical significance of the design variables was determined. A design variable is termed 'significant' if its *p*-value is less than a pre-specified threshold, known as the significant level. In this study, the significant level is 0.05 [22]. Consequently, the shoe width is significant to the mean and approximated variance values of the amplitude of the 16th order AHC. For the mean and approximated variance values of the amplitude of the 144th NHC, the PM eccentricity is significant. Therefore, the shoe width and PM eccentricity are selected as the significant design variables for the RDO.

TABLE VI
DESIGN REQUIREMENTS

Contents		Unit	Value
Rated operating point	Output power	(W)	452
	Speed	(rpm)	2000
Electrical requirements	DC link voltage	(V)	48
Cogging torque's amplitude	Mean	(mNm)	≤ 91.0
	Approximated variance	(mNm^2)	≤ 276.2

TABLE VII
BOUNDARIES OF DESIGN VARIABLES AND DESIGN PARAMETERS

Contents		Unit	min.	Max.
Design variables	Shoe width	(mm)	8.7	9.7
	PM eccentricity	(mm)	0.0	18.8
Design parameters with uncertainties	Semi-minor axis length of stator inner trajectory	(mm)	0.00	0.15
	Out of roundness of stator inner trajectory	(mm)	0.00	0.15

V. ROBUST DESIGN OPTIMIZATION

When manufacturing the segmented stator, avoiding the stator tolerances is difficult. These tolerances may cause a high cogging torque in the SPMSM for robotic actuator, and motion control of the robot may deteriorate. Thus, an RDO is widely used in motor designing [23]–[25]. In this study, the RDO was conducted to determine the robust optimum design model that ensures a small cogging torque even if tolerances are produced in the segmented stator. The proposed modeling method for the segmented stator described in Section II was applied, and the approximated variance defined in Section III was employed to evaluate the cogging torque variation. In this section, an appropriate objective function and constraint are first defined, considering the cogging torque and the electrical requirements for the inverter. Then, the construction of kriging surrogate models by employing the FEA simulations is described. The responses needed for the objective function and constraint were predicted using the kriging surrogate models. Finally, the robust optimum design model was determined.

A. Design Requirements and General Formulation of RDO

The design specifications of the SPMSM for the robotic actuator are presented in Table VI. Regardless of whether the stator tolerances are produced, the amplitude of the cogging torque must be small. Thus, the values of the mean and approximated variance of the cogging torque amplitude were included in the objective function. In addition, the maximum DC link voltage was considered as a constraint. The general formulation of the RDO in this study is presented as:

$$\underset{\mathbf{b}\in R^n}{\text{minimize}}\ F(\mathbf{b}) = w_1 \cdot \frac{{\sigma_f}^2(\mathbf{b},\mathbf{P})}{\max({\sigma_f}^2)} + w_2 \cdot \frac{\mu_f(\mathbf{b},\mathbf{P})}{\max(\mu_f)}$$
$$\text{subject to } G(\mathbf{b}) = \mu_v(\mathbf{b},\mathbf{P}) \le 48, \quad 0 \le \mathbf{b} \le 1 \tag{5}$$

where **b** denotes the vector of the normalized design variables. **P** is the vector of the normalized design parameters with uncertainties. *F* is the objective function of simultaneously minimizing the approximated variance and the mean values of the cogging torque amplitude. ${\sigma_f}^2$ and μ_f is the approximated variance and the mean values of the cogging torque amplitude, respectively. Both ${\sigma_f}^2$ and μ_f are normalized by dividing them with their respective maximum values. In addition, w_1 and w_2 are their corresponding weighting factors. *G* is the constraint that the input voltage must be less than the maximum DC link voltage of 48V.

B. Kriging Surrogate Model

Kriging is an interpolation model using spatial correlation data. Owing to its accuracy for nonlinear functions and high prediction capability, the kriging surrogate model is widely used for design optimization of electric machines [26], [27]. The two significant design variables determined in Section IV and the two design parameters with uncertainties related to the elliptical modeling in Section II were used. Their boundaries are presented in Table VII. To predict the responses in (5), kriging surrogate models were built for the cogging torque amplitude and the input voltage. By using the kriging surrogate model of the cogging torque amplitude, the approximated variance was calculated based on (2)-(4). Then, the mean value of the cogging torque amplitude was predicted when the design parameters are the mean values.

As a sampling strategy for the kriging surrogate models, Latin hypercube design (LHD) was employed. The objective of the LHD is to obtain sample points exhibiting non-collapsing properties in the entire design domain [28]. In this study, 70 sample points using the LHD were selected. Following each of the LHD points, FEA models were constructed, and the voltages and cogging torques were computed. Then, the kriging surrogate models were constructed. A Gaussian correlation function was adopted and its parameters were determined based on the maximum likelihood estimate [29].

As the kriging surrogate models are interpolation models, the responses calculated from such models can differ from the FEA simulation results. Thus, the accuracies of the constructed kriging surrogate models must be evaluated. In this study, the evaluation was based on the leave-one-out cross-validation method [30]. The normalized root mean square error (NRMSE) of a kriging surrogate model is defined as:

$$\text{NRMSE} = \sqrt{\frac{1}{n_s} \cdot \sum_{i=1}^{n_s} \left(\frac{Y(x_i) - \hat{Y}^{(-i)}(x_i)}{\max\{\mathbf{Y}(\mathbf{x})\} - \min\{\mathbf{Y}(\mathbf{x})\}} \right)^2} \cdot 100\% \tag{6}$$

where **x** denotes the vector of inputs, which are design variables and parameters. **Y(x)** denotes the vector of a response's values, which can be cogging torque amplitude or voltage. n_s denotes the number of sample points. x_i denotes the input value at *ith* sample point, and $Y(x_i)$ denotes the response at *i*th sample point calculated from the FEA simulation. $\hat{Y}^{(-i)}(x_i)$ represents the predicted response at the *i*th sample point from the kriging surrogate model which was constructed using sample points except

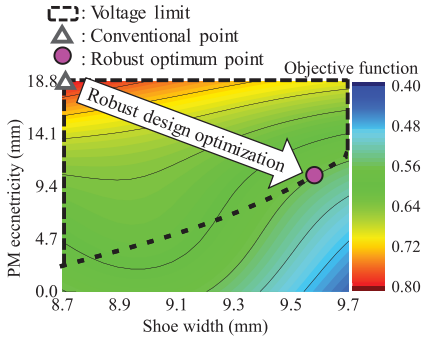

Fig. 8. Objective function with respect to the design variables.

TABLE VIII
DESIGN RESULTS USING KRIGING SURROGATE MODEL

Contents		Unit	Conventional model	Robust optimum design model
Design variables	Shoe width	(mm)	8.7	9.6
	PM eccentricity	(mm)	18.8	10.0
Cogging torque's amplitude	Mean	(mNm)	91.0	67.4
	Approximated variance	(mNm^2)	276.2	110.8

$(x_i, Y(x_i))$. The NRMSEs of the kriging surrogate model for the cogging torque amplitude and voltage were calculated as 7.3%, and 5.0%, respectively, which are considered sufficiently accurate.

C. Robust Design Optimization

Fig. 8 shows the objective function depending on the two design variables: the shoe width and the PM eccentricity. The black dashed line represents the voltage limit. The robust optimum point was selected where the value of the objective function was minimal within the constrained condition. The existing sequential quadratic programming was employed as the optimization method; it is one of the methods that have been successfully developed and used for solving nonlinear constrained optimization problems [31], [32]. The responses for the objective function and the constraint were predicted through the kriging surrogate models, and the cogging torque variation was evaluated with the approximated variance. Thus, only few seconds are required to conduct the RDO.

VI. DESIGN RESULTS AND VERIFICATION

The design results for the robust optimum design model are presented in Table VIII. Compared with the conventional model, the mean and approximated variance values of the cogging torque amplitude are reduced simultaneously in the robust optimum design model; by 25.9% and 59.9%, respectively.

To demonstrate the validity of the RDO results within the same range of the design parameters with uncertainties as those in the conventional model, MCS involving 10^6 simulations was conducted by using the kriging surrogate model. Fig. 9 shows the MCS results of the conventional and robust optimum design

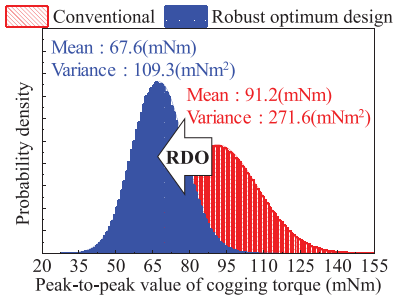

Fig. 9. Cogging torque distribution based on Monte Carlo simulation.

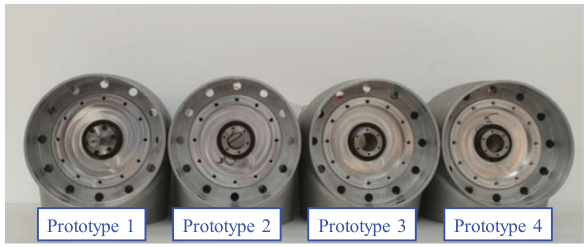

(a) Four prototypes of the robust optimum design model.

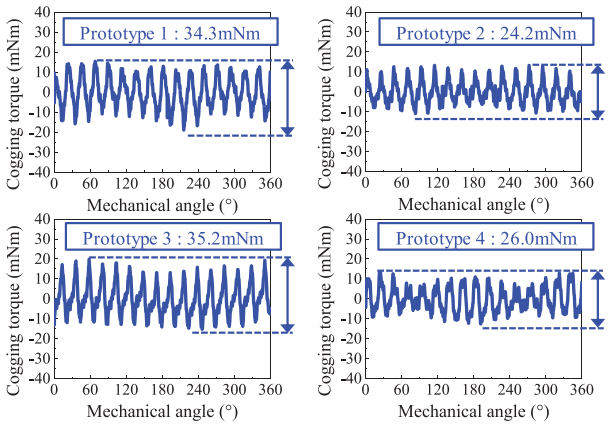

(b) Cogging torque waveforms of the four prototypes. (Test results.)

Fig. 10. Cogging torque test for the robust optimum design model.

models. Similar to the approximated variances, the MCS variance of the robust optimum design model decreased by 59.8% than that of the conventional model. In addition, the lower and upper boundaries of the peak-to-peak values of the cogging torque of the robust optimum design model were approximately estimated; the values of the lower and upper boundaries were estimated as 23mNm and 119mNm, respectively.

For testing the cogging torque test in the robust design optimum model, four prototypes were fabricated, as shown in Fig. 10(a). In all the prototypes, the stator's inner radii were assumed to be within the considered size range, which was sufficiently wide. Fig. 10(b) shows the test results of the cogging torque of the four prototypes for the robust optimum design model. The peak-to-peak values of cogging torque in the four prototypes were within the ranges estimated by the MCS.

These test results were then compared with the cogging torque test result of the conventional model. Figs. 11(a) and (b) show

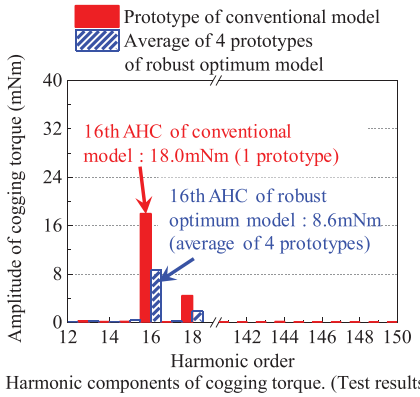

(a) Harmonic components of cogging torque. (Test results.)

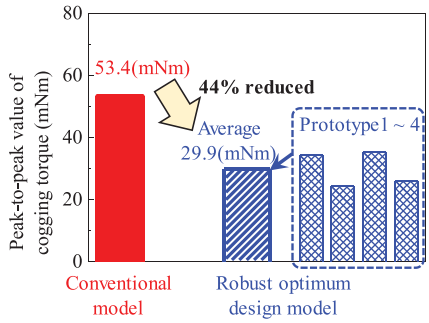

(b) Peak-to-peak values of cogging torque. (Test results.)

Fig. 11. Comparison between the conventional model and the robust design optimum model. (Test results.).

HCs the peak-to-peak values of the tested cogging torque. As the RDO was conducted to reduce the effects of the stator assembly imperfection, the 16th order AHC in the robust optimum design model was less than that in the conventional model. Accordingly, the peak-to-peak values of the cogging torque of the robust optimum design model were reduced compared with that in the conventional model. For the robust optimum design model, the average peak-to-peak value of the four prototypes was 29.9mNm, which shows a decrease of up to 44% compared with the conventional model. Therefore, the validity of the robust optimum design model was verified using the MCS and the cogging torque tests.

VII. Conclusion

In this study, we analyzed the effect of the assembly imperfection of stator segments on the cogging torque variation and proposed a robust design with respect to the cogging torque of the SPMSM as a robotic actuator. An elliptical modeling for the segmented stator was proposed, considering the interconnected structure of the stator segments. Then, the variation in the cogging torque amplitude owing to the stator assembly imperfection was formulated as the approximated variance. By proposing a sensitivity analysis method, the design variables that significantly affected the cogging torque variation were statistically identified. To reduce this variation, sensitivity-based design optimization employing kriging surrogate models were conducted. As a result, the robust optimum design model was determined. To verify the validity of this model, MCS was conducted and the probability distributions of the cogging torque amplitude were estimated. Compared with the conventional model, the mean and the variance values of the probability distribution of the cogging torque amplitude in the robust design optimum model were reduced. Four prototypes were fabricated for the robust optimum design model, and comparisons were conducted with the cogging torque range estimated using the MCS. The cogging torque test results of the four prototypes were within the estimated range. Thus, by using the proposed methods and procedures in this study, the developed robust design is feasible and is less affected by the manufacturing tolerances that occur during mass production of motors.

References

[1] B. Rouzbeh, G. M. Bone, G. Ashby, and E. Li, "Design, implementation and control of an improved hybrid pneumatic-electric actuator for robot arms," *IEEE ACCESS*, vol. 7, pp. 14699–14713, Jan. 2019.

[2] Y. Z. Li, S. J. Zhu, Y. Li, and Q. Lu, "Temperature prediction and thermal boundary simulation using hardware-in-loop method for permanent magnet synchronous motors," *IEEE/ASME Trans. Mechatronics*, vol. 21, no. 1, pp. 276–287, Jun. 2015.

[3] N. J. Baker, D. J. B. Smith, M. C. Kulan, and S. Turvey, "Design and performance of a segmented stator permanent magnet alternator for aerospace," *IEEE Trans. Energy Convers.*, vol. 33, no. 1, pp. 40–48, Mar. 2018.

[4] Z. Q. Zhu, "Influence of design parameters on cogging torque in permanent magnet machines," *IEEE Trans. Energy Convs.*, vol. 15, no. 4, pp. 407–412, Dec. 2000.

[5] V. Hayward and K. E. Maclean, "Do it yourself haptics: Part 1," *IEEE Robot. Automat. Mag.*, vol. 14, no. 4, pp. 88–104, Dec. 2007.

[6] G. Liu and A. A. Goldenberg, "Robust control of robot manipulators incorporating motor dynamics," in *Proc. IEEE/RSJ Int. Conf. Intell. Robots Syst.*, Yokohama, Japan, 1993, pp. 68–75.

[7] W. S. Newman and J. J. Patel, "Experiments in torque control of the adept one robot," in *Proc. IEEE Int. Conf. Robot. Automat.*, 1991, pp. 1867–1872.

[8] J. Y. Lee, J. H. Chang, D. H. Kang, S. I. Kim, and J. P. Hong, "Tooth shape optimization for cogging torque reduction of transverse flux rotary motor using design of experiment and response surface methodology," *IEEE Trans. Magn.*, vol. 43, no. 4, pp. 1817–1820, Mar. 2007.

[9] L. Hao, M. Lin, D. Su, W. Zhang, and N. Li, "Rotor design techniques for reducing the cogging torque in a novel dual-rotor axial field flux-switching permanent magnet machine," in *17th Int. Conf. Elect. Mach. Syst.*, Hangzhou, China, 2014, pp. 1581–1586.

[10] M. S. Islam, S. Mir, and T. Sebastian, "Issues in reducing the cogging torque of mass-produced permanent-magnet brushless DC motor," *IEEE Trans. Ind. Appl.*, vol. 40, no. 3, pp. 813–820, May/Jun. 2004.

[11] L. Gašparin, A. Černigoj, S. Markič, and R. Fišer, "Additional cogging torque components in permanent-magnet motors due to manufacturing imperfections," *IEEE Trans. Magn.*, vol. 45, no. 3, pp. 1210–1213, Mar. 2009.

[12] J. Ou, Y. Liu, R. Qu, and M. Doppelbauer, "Experimental and theoretical research on cogging torque of PM synchronous motors considering manufacturing tolerances," *IEEE Trans. Ind. Electron.*, vol. 65, no. 5, pp. 3772–3783, May 2018.

[13] J. Yuan, C. W. Shi, and J. X. Shen, "Analysis of cogging torque in surface-mounted permanent magnet machines with segmented stators," in *17th Int. Conf. Elect. Mach. Syst.*, Hangzhou, China, 2014, pp. 2513–2516.

[14] Z. Q. Zhu, Z. Azar, and G. Ombach, "Influence of additional air gaps between stator segments on cogging torque of permanet-magnet machines having modular stators," *IEEE Trans. Magn.*, vol. 48, no. 6, pp. 2049–2055, Jun. 2012.

[15] J. M. Kim, M. H. Yoon, J. P. Hong, and S. I. Kim, "Analysis of cogging torque caused by manufacturing tolerances of surface-mounted permanent magnet synchronous motor for electric power steering," *IET Elect. Power Appl.*, vol. 10, no. 8, pp. 691–696, Sep. 2016.

[16] M. F. Momen and S. Datta, "Analysis of flux leakage in a segmented core brushless permanent magnet motor," *IEEE Trans. Energy Conv.*, vol. 24, no. 1, pp. 77–81, Mar. 2009.

[17] X. Ge and Z. Q. Zhu, "Influence of manufacturing tolerances on cogging torque in interior permanent magnet machines with eccentric and sinusoidal rotor contours," *IEEE Trans. Ind. Appl.*, vol. 53, no. 4, pp. 3568–3578, Jul.–Aug. 2017.

[18] X. Ge and Z. Q. Zhu, "Sensitivity of manufacturing tolerances on cogging torque in interior permanent magnet machines with different slot/pole number combinations," *IEEE Trans. Ind. Appl.*, vol. 53, no. 4, pp. 3557–3567, Jul.–Aug. 2017.
[19] R. Y. Rubinstein and D. P. Kroese, "Random number, random variable, and stochastic process generation" in *Simulation and the Monte Carlo Method*. 3nd ed., Hoboken, NJ, USA: Wiley & Sons, 2016, pp. 49–90.
[20] K. H. Lee and D. H. Kang, "A robust optimization using Kriging based approximation model," *JSME. Internat. Journ.*, vol. 49, no. 3, pp. 779–788, 2006.
[21] G. J. Park, T. H. Lee, K. H. Lee, and K. H. Hwang, "Robust design: An overview," *AIAA J.*, vol. 44, no. 1, pp. 181–191, Jan. 2006.
[22] D. C. Montgomery, "Simple comparative experiments," in *Design and Analysis of Experiments*, 9th ed., vol. 2, New York: J. Wiley & Sons, 2017, pp. 23–63.
[23] H. G. Beyer and B. Sendhoff, "Robust optimization–A comprehensive survey," *Comput. Methods Appl. Mech. Eng.*, vol. 196, no. 33–34, pp. 3190–3218, Jul. 2007.
[24] A. Salimi and D. A. Lowther, "On the role of robustness in multi-objective robust optimization: Application to an IPM motor design problem," *IEEE Trans. Magn.*, vol. 52, no. 3, Oct. 2015, Art. no. 8102304.
[25] M. A. Islam, A. Arafat, S. S. R. Bonthu, and S. D. Choi, "Design of a robust five-phase ferrite-assisted synchronous reluctance motor with low demagnetization and mechanical deformation," *IEEE Trans. Energ. Conv.*, vol. 34, no. 2, pp. 722–730, Jun. 2019.
[26] L. Lebensztajn, C. A. R. Marretto, M. C. Costa, and J. L. Coulomb, "Kriging: A useful tool for electromagnetic device optimization," *IEEE Trans. Magn.*, vol. 40, no. 2, pp. 1196–1199, Apr. 2004.
[27] B. Xia, Z. Ren, and C. S. Koh, "Utilizing Kriging surrogate models for multi-objective robust optimization of electromagnetic devices," *IEEE Trans. Magn.*, vol. 50, no. 2, Feb. 2014, Art. no. 7017104.
[28] J. Sacks, W. J. Welch, T. J. Mitchell, and H. P. Wynn, "Design and analysis of computer experiments," *J. Stat. Sci.*, vol. 40, no. 4, pp. 409–423, Nov. 1989.
[29] T. H. Lee and J. J. Jung, "Kriging meta model based optimization," in *Optimization of Structural and Mechanical Systems*, vol. 16, Singapore, Singapore: World Scientific Publishing Co., 2007, pp. 445–484.
[30] N. V. Queipo, R. T. Haftka, W. Shyy, T. Goel, R. Vaidyanathan, and P. K. Tucker, "Surrogate-based analysis and optimization," *Prog. Aeros. Sci.*, vol. 41, no. 1, pp. 1–8, Jan. 2005.
[31] J. Zhang, H. Zhu, S. Q. Zhou, and C. S. Zhao, "Optimal design of a rod shape ultrasonic motor using sequential programming and finite element method," *Finite Elements Anal. Des.*, vol. 59, pp. 11–17, 2012.
[32] P. T. Boggs and J. W. Tolle., "Sequential quadratic programming," *Acta Numerica*, vol. 4, pp. 1–5, 1995.

Soo-Gyung Lee received the bachelor's degree in electrical engineering from Konkuk University, Seoul, South Korea, in 2014. She is currently working toward the Ph.D. degree in automotive engineering with Hanyang University, Seoul, South Korea. Her research interests include the design and optimization of electric machines.

Saekyeol Kim received the bachelor's degree in mechanical engineering and the master's degree in automotive engineering from Hanyang University, Seoul, South Korea, in 2014 and 2016, respectively. His research interests include reliability design optimization, surrogate modeling, uncertainty quantification, statistical model calibration and validation, design optimization of electrical machines and drives.

Jin-Cheol Park received the bachelor's degree in electrical engineering from Chungbuk National University, Cheongju, South Korea, in 2015, and the master's degree in automotive engineering from Hanyang University, Seoul, South Korea, where he is currently working toward the Ph.D. degree. His research interests include the design and analysis of electric machines.

Min-Ro Park received the bachelor's degree in electrical engineering from Chungnam National University, Daejeon, South Korea, in 2013 and the integrated master's and Ph.D. degrees in automotive engineering from Hanyang University, Seoul, South Korea, in 2020. Since 2020, he has been with Korea Institute of Robotics and Technology Convergence (KIRO), Pohang, South Korea, where he is currently a Senior Researcher. His research interests include multiphysics analysis and design of electric machine for mechatronics systems.

Tae Hee Lee (Member, IEEE) is currently a Professor a with the Department of Automotive Engineering, Hanyang University, Seoul, South Korea. He serves the Executive Vice President of KSCM, General Council of IACM and Executive Committee of ASSMO. He received awards for Academic Excellence in Mechanical Engineering (2013) and in CAE and Applied Mechanics (2016) from KSME, and KSCM Computational Mechanics Award (2018). He was a Semi-Plenary Lecturer of WCCM XII (2016) and APCOM VII (2019). His research interests include design optimization, design under uncertainty, surrogate model-based optimization, design and analysis of computer experiments, and data-driven design.

Myung-Seop Lim (Member, IEEE) received the bachelor's degree in mechanical engineering, and the master's and Ph.D. degrees in automotive engineering from Hanyang University, Seoul, South Korea, in 2012, 2014, and 2017, respectively. From 2017 to 2018, he was a Research Engineer with Hyundai Mobis, Yongin, South Korea. From 2018 to 2019, he was an Assistant Professor with Yeungnam University, Daegu, South Korea. Since 2019, he has been with Hanyang University, where he is currently an Assistant Professor. His research interests include electromagnetic field analysis and electric machinery for mechatronics systems, such as automotive and robot applications.